Use of organic materials in dye-sensitized solar cells

Chuan-Pei Lee[1,3], Chun-Ting Li[1,3] and Kuo-Chuan Ho[1,2,*]

[1] Department of Chemical Engineering, National Taiwan University, Taipei 10617, Taiwan
[2] Institute of Polymer Science and Engineering, National Taiwan University, Taipei 10617, Taiwan

In the last two decades, dye-sensitized solar cells (DSSCs) have attracted more attention as an efficient alternative to economical photovoltaic devices, and the highest efficiency record has increased from ~7% to ~14%. To be more competitive in the solar cell markets, various organic materials are investigated and used in DSSCs to improve the cell efficiency, enhance the cell durability, and reduce the cost of production. In this review article, we provide a short review on the organic materials used for the preparation of photoanodes (including metal element-free organic dye sensitizers), quasi/all-solid-state electrolytes, and metal element-free electrocatalytic films in DSSCs with the cell efficiencies of >5%. Finally, the future perspectives for DSSCs are also briefly discussed.

Introduction

In 1991, Professor Grätzel *et al.* made a breakthrough (~7% cell efficiency) on dye-sensitized solar cells (DSSCs) [1], thus facilitating the intensive investigation on this type of solar cells, which were considered as one of the most potential renewable power sources because of their remarkable advantages such as simple fabrication processes in ambient conditions, semi-transparent and colorful appearances, possible plasticity, and high efficiencies (especially under indoor illumination or dim-light irradiation). Figure 1a shows the statistical graph of the number of publications related to the DSSCs over the past two decades (1996–2016). The number of reports on DSSCs was rather limited before 1999; however, DSSCs gained wide attention when the cell efficiency of DSSCs of >10% was reported after 2000 [2,3]; thus, the number of studies on DSSCs has rapidly increased. In 2014, the DSSC with the zinc porphyrin dye and Co[(II/III)] tris(bipyridine)-based redox electrolyte reached an excellent efficiency record of 13.00% [4], and soon after, the highest efficiency record of 14.30% was achieved by a DSSC with the co-sensitization of two metal-free organic dyes and Co[(II/III)] tris(phenanthroline)-based redox electrolyte in 2015 [5]. These breakthroughs further encouraged

research studies on developing economical photovoltaic devices based on DSSCs and rendered DSSCs to be more competitive in the solar cell markets.

As shown in Fig. 1b, a typical DSSC consists of a mesoporous photoanode with dye-sensitized titanium dioxide (TiO_2) film, an electrolyte containing iodide/triiodide (I^-/I_3^-) redox couple, and a counter electrode with platinum (Pt) catalyst. In brief, the basic sequence of events in a DSSC is as follows:

Activation

$$TiO_2/Dye \rightarrow TiO_2/Dye^* \qquad (1)$$

Electron injection

$$TiO_2/Dye^* \rightarrow TiO_2/Dye^+ + e^-(TiO_2) \qquad (2)$$

$$e^-(TiO_2) \rightarrow e^-(FTO) \qquad (3)$$
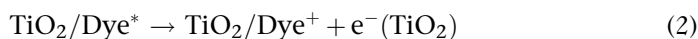
Electron reception

$$I_3^- + 2e^-(Pt) \rightarrow 3I^- \qquad (4)$$

Interception reaction

$$1.5I^- + TiO_2/Dye^+ \rightarrow 0.5I_3^- + TiO_2/Dye \qquad (5)$$
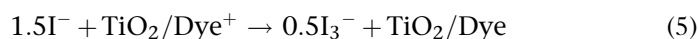
Upon the absorption of light energy, a photo-excited electron is injected from the excited state of the dye (Dye*) into the

*Corresponding author:. Ho, K.-C. (kcho@ntu.edu.tw)
[3] Authors in equal contribution.
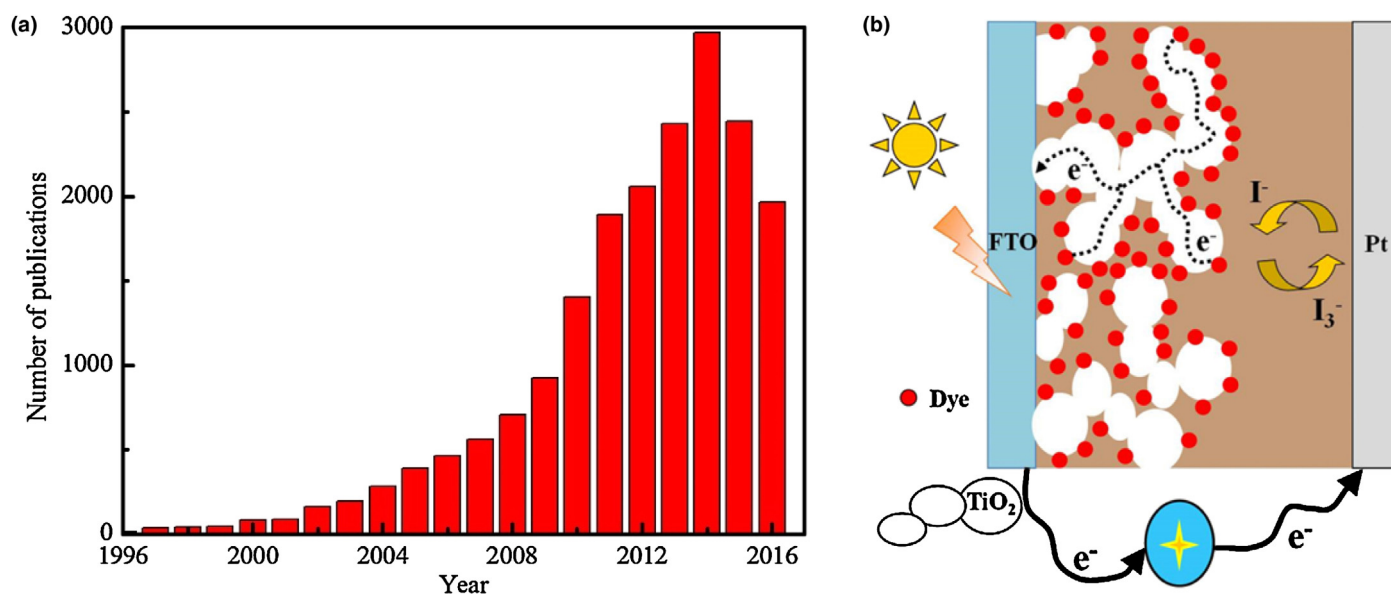
FIGURE 1

(a) A statistical graph of the number of publications related to the DSSCs over the past two decades (1996–2016). Data were obtained from the Scopus database (using title, abstract, and keyword searches for all types of literature studies: dye solar cell). (b) Schematic sketch of a DSSC.

conduction band of the TiO_2. The injected electron percolates through the TiO_2 film by a driving chemical diffusion gradient and is collected at a transparent conductive layer of fluorine-doped tin oxide (FTO) glass substrate, on which the TiO_2 film is formed. After passing through an external circuit, the electron is reintroduced into the DSSC at the Pt CE, where I_3^- is reduced to I^-. Immediately, I^- regenerates the oxidized dye (Dye^+) to complete the circle of a DSSC and to refresh the DSSC without other chemical side reactions. According to the abovementioned working principles of DSSCs, it is clear that each part (i.e., dye-sensitized TiO_2 photoanode, electrolyte, and counter electrode) plays an important role to achieve an efficient DSSC [1].

To effectively improve DSSC performance and reduce its fabrication costs, various organic materials have been investigated to increase the cell efficiency, enhance the cell durability, and reduce the production cost [6]. For photoanode preparation (Section 'New design in photoanodes'), some organic materials of polymers and carbonaceous materials are largely used to develop the efficient mesoporous TiO_2 nanocrystal films (Section 'Mesoporous TiO_2 films'), while other photo-sensitive organic dyes are extensively designed to achieve high solar-to-electricity conversion efficiencies (Section 'Dye sensitizers'). For electrolyte preparation (Section 'Novel development in electrolytes'), organic materials of polymer gelators (Section 'Polymer gelator-based electrolytes') and ionic liquids (Section 'Ionic liquid-based electrolytes') were used to compose the solid-state or quasi-solid-state electrolyte, which aimed to improve the long-term stability of the DSSCs. For counter electrode preparation (Section 'Advanced evolution in counter electrodes'), organic materials of conducting polymers (Section 'Conducting polymer-based counter electrodes') and carbon materials (Section 'Carbonaceous-based counter electrodes') were used to replace the traditional noble metal of Pt. By using the above-mentioned organic materials for DSSC fabrication, the advantage on low costs could facilitate the future industrialization of DSSCs

and would heighten the competitiveness of DSSCs in the solar cell markets. In this article, we present an overview on the organic materials used for the preparation of photoanodes (with organic dye sensitizers), quasi/all-solid state electrolytes, and metal-free counter electrodes in DSSCs with the cell efficiencies of at least >5%; other materials containing any metal element for DSSCs are excluded. Finally, the future perspectives for DSSCs are also briefly discussed.

New design in photoanodes

The reason for the breakthrough for DSSCs in 1991 [1] was the introduction of a mesoporous metal oxide film sensitized with dye molecules as the photoanode; the mesoporous metal oxide film offered high-specific surface area for dye loading, while the dye molecule possessed the broad absorption covering the visible region or even the part of the near-infrared region. Although many types of metal oxide films have been investigated to be used as the photoanode in DSSCs, TiO_2 nanocrystal remains the most popular one because it gave the best performance to the DSSCs and its advantages of low cost, earth abundance, nontoxicity, biocompatibility, and chemically stable nature. However, the following three key issues were encountered during the preparation of an efficient mesoporous TiO_2 nanocrystal film: (1) the poor dispersion or the severe aggregation of TiO_2 nanoparticles, (2) the limited utilization of solar light at long wavelength, and (3) the low-inherent conductivity of the TiO_2 film. Therefore, organic materials of polymers and carbonaceous materials were used to obtain the mesoporous TiO_2 nanocrystal film with moderate pore size, good light-scattering property, and electrical conductivity. In addition to the TiO_2 nanocrystal film, the dye sensitizers in the photoanode of DSSCs play the role of the absorber for converting solar energy into electric power. Because the commonly used dyes of ruthenium (Ru) bipyridyl derivatives (N3: cis-diisothio-cyanato-bis(2,2′-bipyridyl-4,4′-dicarboxylic acid) ruthenium(II);

TABLE 1

A partial list of literature studies on the DSSCs with TiO$_2$ films prepared using various organic materials.

Organic materials for the preparation of TiO$_2$ film	Redox couple	Dye	η (%)	Ref.
Organic materials for TiO$_2$ film: polymer dispersant type				
PEG	I$^-$/I$_3^-$	N3	5.31	[8]
PEG	I$^-$/I$_3^-$	N719	5.65	[9]
AESO	I$^-$/I$_3^-$	N719	7.30	[11]
MAESO	I$^-$/I$_3^-$	N719	9.00	[11]
Organic materials for TiO$_2$ film: polymer template type				
PVC-g-POEM	I$^-$/I$_3^{-a}$	N719	5.00	[12]
PLMA–POEM	I$^-$/I$_3^{-a}$	N719	5.00	[18]
PBEM–POEM	I$^-$/I$_3^{-a}$	N719	6.60	[19]
PS spheres	I$^-$/I$_3^-$	N3	6.70	[20]
PMMA spheres	I$^-$/I$_3^-$	N3	5.81	[21]
Organic materials for TiO$_2$ film: carbonaceous conductive channel type				
MWCNT	I$^-$/I$_3^-$	N3	5.02	[22]
MWCNT	I$^-$/I$_3^-$	N719	10.29	[23]
SWCNT	I$^-$/I$_3^-$	N. A.	N. A.	[24]
Graphene	I$^-$/I$_3^-$	N3	6.97	[25]

^{a} Quasi-solid-state electrolyte.

N719: di-tetrabutylammonium cis-bis(isothiocyanato)bis(2, 2'-bipyridyl-4,4'-dicarboxylato) ruthenium(II); Z907: cis-bis (iso-thiocyanato)(2,2'-bipyridyl-4,4'-dicarboxylato)(4,4'-di-nonyl-2'-bipyridyl) ruthenium(II)) had high costs and exhibited low extinction coefficients, the metal-free organic dyes were intensively investigated for DSSCs in recent years. Metal-free organic dyes usually have much higher extinction coefficients than those of Ru-dyes, and they can be synthesized and purified in an easier and more economical way than those of Ru-dyes. In this section, we briefly review the developments of the photoanode for the DSSCs with cell efficiencies >5%; the organic materials based on polymers and carbonaceous materials for constructing the mesoporous TiO$_2$ thin films are described in Section 'Mesoporous TiO$_2$ films', while the investigation of the efficient metal-free organic dyes are described in Section 'Dye sensitizers'.

Mesoporous TiO$_2$ films

The mesoporous TiO$_2$ layer plays an important role in collecting photo-excited electrons from the dye molecules and transferring them to the conductive substrate (i.e., FTO) and subsequently to the external circuit. Therefore, the modification of the TiO$_2$ layer has been intensively investigated because of its importance in determining DSSCs' performance. To prepare highly efficient mesoporous TiO$_2$ nanocrystal films, several polymers and carbonaceous materials were used, and these materials can be divided into three types in accordance with their functions: (1) polymer dispersant type, (2) polymer template type, and (3) carbonaceous conductive channel type. All types of these functional materials are briefly reviewed below. The photovoltaic parameters of the corresponding DSSCs with cell efficiencies >5% are summarized in Table 1. The molecular structures of the polymer dispersant type and polymer template type materials are shown in Fig. 2.

Polymer dispersant type

Because the poor dispersion or the severe aggregation of TiO$_2$ nanoparticles in the film could lead to the poor electron transfer and severe charge recombination in the DSSCs due to the unfavorable interfacial contact between the TiO$_2$ film and the

FTO substrate, a mesoporous TiO$_2$ film was usually incorporated with a polymer dispersant such as polyethylene glycol (PEG) [7,8]. Lee et al. prepared two types of TiO$_2$ pastes using PEGs with different molecular weights [MW = 20,000 (P1) and 200,000 (P2)] for constructing various bi-layered TiO$_2$ electrodes for DSSCs. Accordingly, three TiO$_2$ electrodes separately consisted of bi-layered P1/P1, P1/P2, and P2/P2 TiO$_2$ thin films, which were controlled at the identical film thickness. They found that the DSSC with bi-layered P1/P2 TiO$_2$ film shows a better cell efficiency (5.31%) than other cells with bi-layered P1/P1 and P2/P2 TiO$_2$ films; this result revealed the fact that the surface area and pore size for a good TiO$_2$ electrode should be optimized [8]. Yanagida et al. have investigated the performance of DSSCs with the TiO$_2$ electrodes prepared using various amounts of PEG. Their results indicated that the mesoporous TiO$_2$ film prepared with the
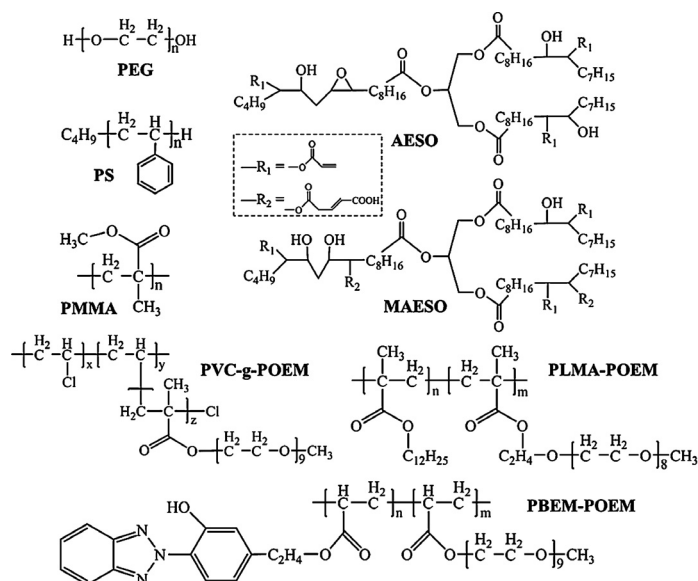
FIGURE 2

The molecular structures of polymers used for preparing the mesoporous TiO$_2$ films.

optimized amount of PEG possesses an average pore size of 15–25 nm, a porosity of 45–55%, a roughness factor about 1400, and thus an optimized cell efficiency of 5.65% [9]. However, the usage of PEG could hinder the electron transport in the TiO$_2$ film because it is difficult to remove thoroughly by sintering; thus, the residual organics would introduce impurity states that trap the photo-excited electrons [10]. Accordingly, Park et al. synthesized chemically functionalized plant oils, namely acrylated epoxidized soybean oil (AESO) and maleinized acrylated epoxidized soybean oil (MAESO), as environmental-friendly dispersants for controlling the morphology of the TiO$_2$ electrodes in DSSCs [11]. When the AESO and MAESO were used for the preparation of the TiO$_2$ electrodes, the conversion efficiency of the corresponding DSSCs was significantly improved to 7.30% and 9.00%, respectively, as compared to that of the cell using PEG (4.60%).

Polymer template type

Because the mesoporous TiO$_2$ films possess the limited utilization of solar light at long wavelength, several reports indicate that the use of an organized mesoporous TiO$_2$ film could effectively enhance the DSSC performance by increasing the transmittance of the transparent TiO$_2$ layer or by improving the light-scattering effect of the TiO$_2$ scattering layer [12–21]. Organized mesoporous metal oxide films are typically prepared using block copolymer-templated synthetic strategies [12–19]. For example, Ahn et al. synthesized the organized mesoporous TiO$_2$ films with high porosity and good connectivity using sol–gel by templating an amphiphilic graft copolymer consisting of poly(vinyl chloride) backbone and poly(oxyethylene methacrylate) side chains, that is, PVC-g-POEM [12]. Introduction of the organized mesoporous TiO$_2$ layer in photoanode resulted in the increased transmittance of the visible light, decreased interfacial resistance, and enhanced electron lifetime. Consequently, the cell efficiency of the pertinent DSSC employing a polymer gel electrolyte was significantly improved from 3.50% to 5.00%. Kim et al. synthesized rubbery amphiphilic comb-like copolymers (coded as PLMA–POEM) consisting of hydrophobic poly(lauryl methacrylate) (PLMA) and hydrophilic poly(oxyethylene methacrylate) (POEM) for constructing the honeycomb-like mesoporous TiO$_2$ films for the DSSC with a polymeric ionic liquid electrolyte [18]. The DSSCs with the honeycomb-like mesoporous TiO$_2$ photoanode exhibited a higher efficiency (5.00%) than that of cell with commercially available TiO$_2$ photoanode (3.90%) due to better pore filling of the quasi-solid-state electrolyte and improved light-scattering properties. Recently, their group (Lee et al.) also developed a new comb copolymer (coded as PBEM–POEM) consisting of hydrophobic poly(2-[3-(2H-benzotriazol-2-yl)-4-hydroxyphenyl] ethyl methacrylate) (PBEM) and hydrophilic poly(oxyethylene methacrylate) (POEM) to fabricate well-organized worm-like mesoporous TiO$_2$ films for the DSSC with a polymeric ionic liquid electrolyte [19]. The introduction of the worm-like TiO$_2$ layer between the TiO$_2$ film and FTO substrate results in the increased transmittance of the visible light and decreased interfacial resistance. Consequently, the efficiency of the corresponding DSSC was increased from 5.30% to 6.60%. In addition to the block copolymer-templated synthetic strategies, several reports used submicrosized polymer spheres as the template to construct the well-organized mesoporous TiO$_2$ film [20,21]. Hore et al. utilized spherical voids as

light-scattering centers in TiO$_2$ films by incorporating polystyrene (PS) particles of diameter 400 nm into TiO$_2$ electrode preparation [20], thus enhancing the corresponding photovoltaic performance by 25% (from 5.40% to 6.70%) and reducing the ionic diffusion resistance in the highly viscous electrolytes (i.e., quasi-solid-state electrolytes). Lee et al. incorporated monodispersed poly(methyl methacrylate) (PMMA) spheres in the TiO$_2$ paste to fabricate a TiO$_2$ film with uniform spherical voids of diameter ∼350 nm for the photoanode in a quasi-solid-state DSSC [21]. Because of the benefits of light-scattering centers and low ionic diffusion resistance, the cell efficiency of the quasi-solid-state DSSC increased from 3.61% to 5.81% by using the PMMA-templated TiO$_2$ film.

Carbonaceous conductive channel type

Because the inherent conductivity of the TiO$_2$ film is still low, the transport of the injected electrons from the TiO$_2$ network to the FTO conductive substrate becomes one of the bottlenecks in photoanode. Recently, many research groups have incorporated one-dimensional carbon nanotubes (CNTs) into TiO$_2$ films as electron transport channels to improve the cell performance. Lee et al. incorporated 0.1 wt% multi-wall carbon nanotubes (MWCNT) into a low-temperature prepared TiO$_2$ photoanode (i.e., the organic binder-free TiO$_2$ film sintering at 150 °C) to enhance the electrical conductivity of the TiO$_2$ film [22]. They found that the pertinent DSSC exhibited a better cell efficiency of 5.02% than that of cell with a pristine TiO$_2$ film (4.15%), which is due to the improvement of the electron lifetime in the 0.1 wt% MWCNT-modified TiO$_2$ photoanode. However, a higher loading of MWCNT causes light-harvesting competition that affects the light absorption of the dye sensitizer and decreases the surface area for dye loading, and consequently reduces the cell efficiency. Meanwhile Sawatsuk et al. also synthesized a MWCNT-modified TiO$_2$ electrode for a DSSC, which reached a remarkable efficiency of 10.29% [23]. Moreover, a single-wall carbon nanotubes (SWCNT)-modified TiO$_2$ film was investigated for the photoanode of DSSCs by Brown et al. [24]. Their report demonstrated that the SWCNT-supported networks can be incorporated into TiO$_2$ films to improve the electron transport in DSSC (i.e., much enhancement on photocurrent density), but no net increase in power conversion efficiency was seen. In their study, SWCNT acts as a conducting scaffold to facilitate charge separation and charge transport in TiO$_2$ films. On the other hand, two-dimensional graphene nanomaterials have also been proven to be an attractive candidate for improving the performance of the TiO$_2$ photoanodes in DSSCs. Yang et al. introduced graphene as two-dimensional bridges into the TiO$_2$ electrodes of DSSCs, which brought a faster electron transport and a lower recombination, together with a higher light-scattering [25]. Their study showed that the photocurrent density of the DSSC with graphene-modified TiO$_2$ electrode was increased by 45%, and the total conversion efficiency (6.97%) was increased by 39% as compared to that of the cell with pristine TiO$_2$ electrode (5.01%), and it was obviously much better than that of the cell with CNT-modified TiO$_2$ electrode (0.58%).

Dye sensitizers

In a DSSC, a dye sensitizer plays a very important role in generating the photo-induced electrons and injecting them into the

conduction band of the TiO_2 semiconductor. An ideal dye sensitizer for DSSCs should meet several criteria of (1) absorbing solar light below a threshold wavelength of ~920 nm, (2) being strongly grafted to the TiO_2 surface, (3) smoothly injecting electrons to the conduction band of TiO_2 semiconductor, (4) having suitable redox potential that can be rapidly regenerated through the redox couple (I^-/I_3^-) in the electrolyte, and (5) being stable under solar light illumination and continuous light soaking. According to these criteria, the efficient dye sensitizers can be simply divided into two groups: (1) metal complex dyes and (2) metal-free organic dyes [26,27]. Although the metal complex dyes have achieved the high-conversion efficiency (η) up to 13.0% [4], the high costs, complicated synthesis routes, and the limited extinction coefficients in the visible region of metal complex dyes have confined their developing potentials in the DSSCs. Because the DSSC co-sensitized with two metal-free organic dyes reached the highest record of 14.3% [5], metal-free organic dyes are considered as the promising materials to replace the metal complex dyes, and have been extensively explored for DSSCs due to their simple synthesis, economical purification, easy for large-scale production, good flexibility in molecular design, and extremely high molar extinction coefficients (usually $>2.50 \times 10^4 \, M^{-1} \, cm^{-1}$ in the visible region) of the charge transfer band [28]. Moreover, compared to the metal complex dyes, the higher extinction coefficient of organic dyes allows the use of much thinner TiO_2 films; thereby the energy losses during charge transport in the photoanode can be reduced, and the extent of pore filling for quasi-solid-state and/or solid-state electrolyte in porous dye-sensitized TiO_2 films can be enhanced. Here, the organic dyes were simply divided into two types, including the dyes with (1) the visible light absorption and (2) the near-infrared light absorption; each type of organic dyes is briefly reviewed below. The molecular structures of these dyes are categorized in Fig. 3. The photovoltaic parameters of the corresponding DSSCs adsorbed with the single organic dye are summarized in Table 2. In this section, the organic dyes that reached cell efficiencies >5% are introduced.

Organic dyes with visible light absorption

The organic dyes with visible light absorption usually possess a donor-π-acceptor configuration consisting of an electron donor and an electron acceptor, which are linked covalently through a π-conjugated bridge/spacer [28]. Under light illumination, the photo-induced electrons transport through an intramolecular route in an organic dye: electron donor moiety → π-conjugated bridge/spacer → electron acceptor moiety → anchoring acid ligand, and finally enter the TiO_2 network; this charge transfer phenomenon is generally called the 'electron injection,' which is the heart of solar-to-electricity conversion processes in a DSSC. In an organic dye, the tunable structure of the π-conjugated spacers is a key to influence both the highest occupied molecular orbital and the lowest unoccupied molecular orbital levels, and thereby the photo-physical properties of an organic dye. Thus, we present a brief overview on the organic dyes with the visible light absorption (Fig. 3a) and their DSSCs' performance according to the molecular structures of the π-conjugated spacers, that is, (i) the spacers containing fluorene fragments and (ii) the spacers containing electron-deficient moieties.

Spacers containing fluorene fragments

Zeng et al. reported a C219 dye with a binary π-conjugated spacer of ethylenedioxythiophene and dithienosilole; the function of the binary spacer is to keep the blocks of both lipophilic alkoxyl-substituted triphenylamine and hydrophilic cyanoacrylic acid apart [29]. The DSSC with this amphiphilic C219 dye exhibited an η of 10.10%, which reached an encouraging milestone in the development of organic dyes. Bai et al. synthesized a C229 dye by incorporating the 2,6-bis(thiophen-2-yl)-4,4-dihexyl-4H-cyclopenta[2,1-b:3,4-b']dithiophene as the π-spacer; the pertinent cell exhibits an excellent efficiency of 9.40% with a $Co^{(II/III)}$ tris(bipyridyl)-based electrolyte [30]. Xu et al. synthesized a C218 dye containing dihexyloxy-substituted triphenylamine and gave an η of 9.30% to its cell using a $Co^{(II/III)}$ tris(bipyridyl)-based electrolyte [31]. Lai et al. synthesized a 3C dye with multicarbazole units that exhibited twisted and zigzag-shape structure [32]. The non-planar structure of 3C dye that combined with multiple alkyl chains could efficiently inhibit dye aggregation and charge recombination. The DSSC with 3C dye showed a high open-circuit voltage (V_{OC}) of 796 mV and an η of 6.33%. Chen et al. synthesized a series of organic dyes with polyphenyl-substituted ethylene end-capped groups (i.e., diphenylethylene, triphenylethylene, and tetraphenylethylene), which had a considerable effect on the V_{OC} of the DSSCs; the one with triphenylethylene end-capped group, namely VP3, rendered its cell a high V_{OC} of 789 mV and the best η of 6.29% [33].

Spacers containing electron-deficient moieties

Zhu et al. incorporated the electron-withdrawing entity, benzothiadiazole, in the organic dye (WS-2), which exhibited a broad spectrum with a high plateau at the visible region until 720 nm and an onset at the near-infrared region at about 850 nm [34]. The DSSC with WS-2 and the co-adsorbed deoxycholic acid (DCA) possessed a high η of 8.70%. On the basis of WS-2, two extended dyes of WS-6 [35] and WS-9 [36] were developed by incorporating an n-hexyl chain onto the thiophene unit and by adding an extra n-hexylthiophene unit in the π-conjugated spacer, respectively; the pertinent DSSCs reached 7.76% (without DCA) and 9.04% (with DCA) correspondingly. Qu et al. reported a YCD01 dye, which included the 2-ethyl-hexyl chain in the diketopyrrolopyrroles moiety and rendered its cell a good η of 7.43% with an excellent stability [37]. He et al. synthesized a BT-I dye containing bithiazole motifs to obtain an η of 7.51% [38]. Dessi et al. designed and synthesized a new thiazolo[5,4-d]thiazole-based organic dye containing two propylenedioxythiophene groups, coded as TTZ5, which shows a very high molar extinction coefficient of $9.41 \times 10^4 \, M^{-1} \, cm^{-1}$ at 510 nm [39]. Using TTZ5 dye as the sensitizer and chenodeoxycholic acid (CDCA) as the co-adsorbate, the pertinent cell exhibited a good η of 7.71% with a remarkable J_{SC} of 18.33 mA cm^{-2}. Chou et al. provided a dipolar R4 dye containing a 5,6-bis-hexyloxy-benzo[2,1,3]thiadiazole entity to obtain η of 6.72% [40]. Cui et al. synthesized the indoline-based WS-5 by incorporating benzotriazole unit with octyl group into its π-conjugated spacer; this octyl group shows the good ability to suppress charge recombination and thereby resulted in a good η of 8.02% with a good V_{OC} of 780 mV [41]. Chen et al. used the heteroaromatic ring as the π-conjugated spacer in the organic dye (denoted as 6), which exhibited very high molar extinction
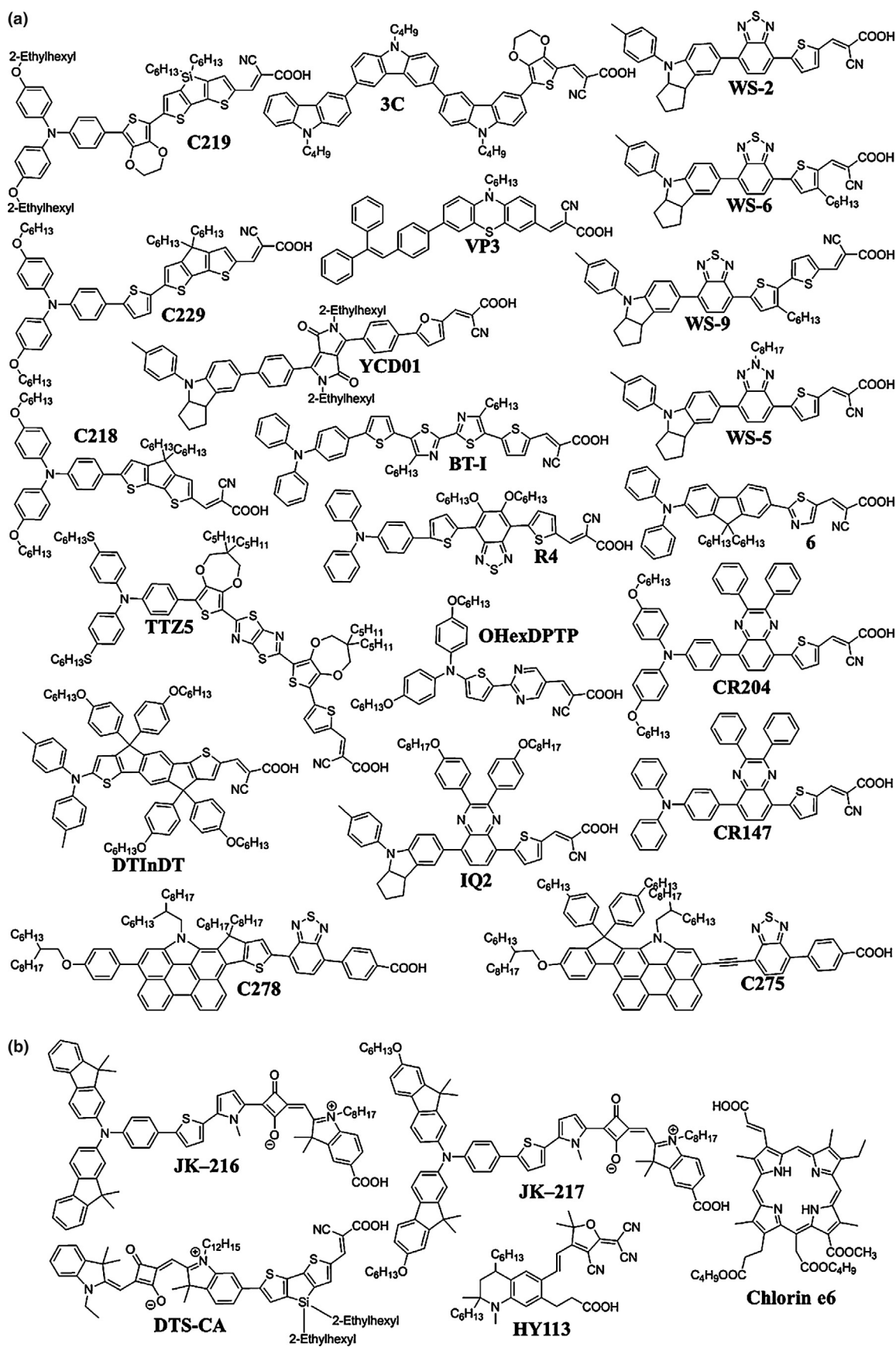
FIGURE 3

The molecular structures of the typical metal-free organic dyes having the absorbance in (a) the visible light region and (b) the near-infrared light region.

TABLE 2

A partial list of literature studies on the DSSCs with metal-free organic dyes.

Metal-free organic dyes	λ_{max} [a] (nm)	Redox couple	η (%)	Ref.
Organic dyes with visible light absorption				
C219	493	I^-/I_3^-	10.10	[29]
C229	575	Co^{2+}/Co^{3+}	9.40	[30]
C218	517	Co^{2+}/Co^{3+}	9.30	[31]
3C	444	I^-/I_3^-	6.33	[32]
VP3	474	I^-/I_3^-	6.29	[33]
WS-2	533	I^-/I_3^-	8.70	[34]
WS-6	547	I^-/I_3^-	7.76	[35]
WS-9	536	I^-/I_3^-	9.04	[36]
YCD01	526	I^-/I_3^-	7.43	[37]
BT-I	470	I^-/I_3^-	7.51	[38]
TTZ5	510	I^-/I_3^-	7.71	[39]
R4	501	I^-/I_3^-	6.72	[40]
WS-5	496	I^-/I_3^-	8.02	[41]
6	448	I^-/I_3^-	6.88	[42]
DTInDT	500	I^-/I_3^-	6.70	[43]
OHexDPTP	506	I^-/I_3^-	7.64	[44]
IQ2	523	I^-/I_3^-	8.50	[45]
CR147	460	I^-/I_3^-	7.35	[46,47]
CR204	447	I^-/I_3^-	6.49	[47]
C278	565	Co^{2+}/Co^{3+}	12.00	[48]
C275	536	Co^{2+}/Co^{3+}	12.50	[49]
Organic dyes with near-infrared light absorption				
JK-216	669	I^-/I_3^-	6.29	[50]
JK-217	672		5.99	
DTS-CA	667	I^-/I_3^-	8.90	[51]
HY113	615	I^-/I_3^-	5.10	[53]
Chlorin e6	N.A.	I^-/I_3^-	6.70	[54]

[a] Wavelength at the absorption maximum (λ_{max}).

coefficient ($5.13 \times 10^4\,M^{-1}\,cm^{-1}$ at 448 nm) to reach an η of 6.88% [42]. Chen et al. reported an indacenodithiophene-based DTInDT dye, which was functionalized with 4-(n-hexoxy)phenyl groups on the sp^3-carbon bridge; an η of 6.70% was obtained [43]. Lin et al. reported the OHexDPTP dye containing an electron-deficient pyrimidine ring to achieve an η of 7.64% [44]. Pei et al. employed the quinoxaline moiety for an electron-withdrawing IQ2 dye to obtain a high η of 8.50% [45]. Because the electron-deficient diphenylquinoxaline moiety can effectively reduce the energy gap and broaden the absorption range of a dye, Li et al. reported two conveniently prepared organic dyes with diphenyl-quinoxaline-based moieties, that is, CR147 [46,47] and CR204 [47], to achieve good η's of 7.35% and 6.49%, respectively. Recently, Professor Wang's group achieved a notable landmark in the progress of organic dyes for DSSCs. They designed a highly efficient and stable metal-free perylene dye, namely C278 [48], which consisted of the electron-acceptor 4-(benzo[c]-[1,2,5]thiadiazol-7-yl)benzoic acid, polycyclic aromatic hydrocarbon segment (N-annulated 13H-thieno[2',3':3,4]cyclopenta[b]perylene), alkoxy-phenyl end-capped group, and aliphatic side-functionalized chains. The DSSC using C278 dye and $Co^{(II/III)}$ tris(bipyridyl)-based electrolyte attained a very high η of 12.00% without the use of any co-adsorbate. Meanwhile they also synthesized another metal-free perylene dye, coded as C275 [49], characterized by the new electron-donor N-annulated indeno[2,1-b]-perylene and electron-acceptor ethynylbenzothiadiazolylbenzoic acid. Without

any co-adsorbate, the C275 dye was used solely to give an impressive η of 12.50% to its DSSC with the excellent V_{OC} and FF of 956 mV and 0.77, respectively.

Organic dyes with near-infrared light absorption

The organic dyes with near-infrared light absorption are designed to improve the solar-to-electricity conversion efficiency by extending the absorption threshold of the organic dyes to the near-infrared regions, which accounts approximately 45% of the total solar energy. Several near-infrared light absorption type organic dyes (Fig. 3b) have been proposed for DSSCs. For example, Paek et al. designed a new series of stable and unsymmetrical squaraine dyes (JK-216 and JK-217) containing both thiophenyl pyrrolyl and indolium groups [50]. Dyes JK-216 and JK-217 have an absorption band at 669 and 672 nm, respectively; and their cells reached the η's of 6.29% and 5.99% correspondingly. Jradi et al. synthesized a new squaraine-based dye (DTS-CA) featuring 4,4-bis(2-ethyl-hexyl)-4H-silolo[3,2-b:4,5-b']dithiophene π-bridges, and cyanoacetic acid acceptor/anchoring group [51]. The DSSC with DTS-CA dye showed an excellent η of 8.90% (with CDCA co-adsorbate), which is the highest reported performance in literature studies for squaraine dyes. Hao et al. reported a new strategy in which the anchoring group is not attached to the acceptor groups of the dyes [52,53]; for example, HY113 [53] dye with such structure containing the long alkyl chains on the donor. The long alkyl chains prevent the dye aggregates on the surfaces of the semiconductor nanoparticles and thereby blocking the charge recombination; thus, a DSSC with HY113 dye showed a maximum IPCE of 93% at 660 nm and an η of 5.10%. Wang et al. designed a chlorophyll derivative-based dye, namely chlorin e6, by introducing alkyl ester substituents at the C15 and C17 positions of the chlorin macro-cycle of chlorin e6 [54]. The cell with chlorin e6 dye exhibited a broad and steady absorption range from 350 to 775 nm and reached a good η of 6.70%.

Novel development in electrolytes

The electrolyte functions as a vital mediator between a photo-anode and a counter electrode in DSSCs. The function of an electrolyte is (1) to regenerate the oxidized dyes at the photo-anode/electrolyte interface using a reduced-state redox species (e.g., iodide (I^-) of iodide/triiodide (I^-/I_3^-), Co^{2+} of Co^{2+}/Co^{3+}, thiolate (T^-) of disulfide/thiolate (T_2/T^-) etc.), (2) to conduct the electricity between a photoanode and a counter electrode using its components of ions/redox species, and (3) to be regenerated by the electro-catalysts at the counter electrode. The electrolyte is a key to maintain the recycling of the DSSCs [55]. In addition, the redox species in an electrolyte offers a redox standard potential, which differs from the Fermi level of the TiO_2 semiconductor; in accordance with this energy-level difference, a value of the open-circuit voltage (V_{OC}) is set to drive the electron flow in a DSSC. The traditional electrolytes used in DSSCs are mostly based on the I^-/I_3^- redox couple, which possess several drawbacks regarding the light absorption in the visible region, corrosion of metal current collectors, sublimation of iodine, and mismatch between the I^-/I_3^- redox potential and the highest occupied molecular orbital level of the sensitizer. Accordingly, some redox active organic compounds, as shown in Fig. 4a, are investigated as the alternative redox couples for the electrolyte of DSSCs. Zhang et al. introduced

a stable organic radical, 2,2,6,6-tetramethyl-1-piperidinyloxy (TEMPO), as the redox mediator for DSSCs, which yielded an η of 5.40% [56]. Wang et al. reported a new disulfide/thiolate (T_2/T^-) redox couple, and the pertinent DSSC exhibited an η of 6.44% [57]. Chen et al. prepared a DSSC using the newly developed L-cysteine/L-cystine redox couple, which showed a comparable efficiency of 7.70%, as compared to the cell using I^-/I_3^- redox couple (8.10%) [58]. Meanwhile they also synthesized a new type of hybrid electrolyte containing the tetramethylammonium hydroquinone (HQ)/benzoquinone (BQ) redox couple. The pertinent DSSC exhibited an efficiency of 8.40%, which is higher than an efficiency of 8.00% based on their standard cell using I^-/I_3^- redox couple [59]. In all cases, however, the presence of organic solvent in the liquid electrolyte would lead to several problems, including the hermetic sealing of the cell, the evaporation of solvents at high temperature, and thereby the lack of long-term stability of a cell. In fact, manufacturing of multicell modules of DSSCs becomes a complex task with a liquid-type electrolyte. Therefore, the developments in the solid-state or quasi-solid-state DSSCs have been intensely studied with various approaches, such as the usages of the electrolytes containing p-type inorganic semiconductors [60], organic hole transporting materials [61], polymer gelator (PG) [62], ionic liquids (IL) [63], etc. CuI or CuSCN inorganic hole transporting materials possess high hole mobility, but their fast crystallization rates result in poor filling into porous TiO_2/dye films, and thus, the corresponding solid-state DSSCs usually showed low η of <4% [64]. Another p-type semiconductor, $CsSnI_3$, was employed as the hole transporting material in DSSCs [65], and the pertinent cell yielded an η of up to 10.20%. However, the inclusion of Cs element would prohibit the widespread use in solar cells due to its hazardous property. Among organic hole transporting materials, Spiro-MeOTAD (Fig. 4b) is much better than the other types (e.g., conducting polymers), and a certified efficiency of 6.08% was achieved for Spiro-MeOTAD-based solid-state DSSCs [66]. However, the high manufacturing costs still prevent the practical application of Spiro-MeOTAD from the solid-state DSSCs. In 2013, the Spiro-MeOTAD hole transporting material in conjunction with perovskite-sensitized solar cells produced a remarkable η of 15.00% [67]. In fact, the first perovskite solar cells belong to DSSCs where the sensitizer and electrolyte layers were replaced by small perovskite particles [68]. This new kind of solar cells have amazed with an incredibly fast efficiency improvement, going from just 3.81% [68] to over 19.30% [69] within few years. Thus far, the highest efficiency record of perovskite solar cells has been enhanced to 21.10% [70]. Nevertheless, they have several disadvantages such as reliance on an environmentally hazardous heavy metal and the low toleration to moist air and water vapor. Therefore, on the aspects of environmental friendly materials and durability issues, the perovskite solar cells are less competitive in green energy markets unless the key issues can be resolved in the future. Accordingly, polymer gelator-based and ionic liquid-based electrolytes (see Fig. 4c and d) are considered as the most prospective substitutes for liquid electrolytes to obtain the long-term sustainable DSSCs; their photovoltaic performances are summarized in Table 3. This fact is because of the merits of high ionic conductivities, favorable pore-filling properties, good long-term stability, and most importantly the leakproof abilities of polymer gelator-based and ionic liquid-based electrolytes. In Sections

'Polymer gelator-based electrolytes' and 'Ionic liquid-based electrolytes', we present a brief overview on the recent developments of polymer gelator-based and ionic liquid-based electrolytes for DSSCs with cell efficiencies >5%, respectively.

Polymer gelator-based electrolytes

The polymer gelators have received a wide attention in recent years owing to the flexible molecular structures tailoring for the noncovalent chelating interaction with ionic species, the formation of the hybrid networks for the fast charge transfer, and the sustainable long-term stability [71,72]. Polymers commonly used for the polymer gelator-based electrolytes include poly(ethylene glycol) (PEG), poly(acrylonitrile) (PAN), poly(methyl methacrylate) (PMMA), poly(vinylidene fluoride) (PVDF), and poly(vinylidenefluoride-co-hexafluoropropylene) (PVDF-HFP), etc. For example, Wu et al. reported a thermoplastic gel electrolyte with an ionic conductivity of 2.61 mS cm^{-2} by adding 40 weight percentage (wt.%) of PEG as the polymeric host in the liquid electrolyte; thus, the pertinent quasi-solid-state DSSC reached an η of 7.22% [62]. Zhang et al. have developed several PEG/PVDF-HFP composites modified by different amounts of NH_2-end functional silanes (3-amonopropyltriethoxysilane, APTS) [73]; an η of 5.08% was obtained using the PEG/PVDF-HFP electrolyte modified by a moderate (0.1 M) APTS content. Lan et al. have developed a closed-microporous hybrid of poly(acrylic acid)-poly(ethylene glycol)-polypyrrole (PAA-PEG-PPy) by the in situ polymerization and the micro-phase separation of PPy in PAA-PEG gel; a good η of 6.30% was obtained [74]. Chen et al. used poly-1,1′-(methylenedi-4,1-phenylene)bismaleimide (PBMI) as the gelator of the liquid-type electrolyte by the in situ polymerization of the corresponding monomer of 1,1′-(methylenedi-4,1-phenylene)bismaleimide (BMI) without an initiator at 30 °C; the pertinent cell exhibited an η of 6.24% [75]. Dong et al. designed a new class of elastomeric type poly(oxyethylene)-segmented amide–imide copolymer (POE–PAI) with a cross-linked structure; this POE–PAI is capable of absorbing the large amount of the liquid electrolyte using its three-dimensional porous channels [76]. When this POE–PAI elastomer absorbed with 76.8 wt% of the liquid electrolyte using 3-methoxypropionitrile (MPN) as a solvent, it rendered its DSSC an η of 9.48%, which is surprisingly superior to that of the cell using the liquid electrolyte (8.84%). This is because of the effective suppression of the back electron recombination using this POE–PAI elastomer. The same research group further allowed this POE–PAI elastomer to absorb liquid electrolytes based on different solvents, including propylene carbonate (PC), dimethylformamide (DMF), and N-methyl-2-pyrrolidone (NMP) [77]. Three POE–PAI-based quasi-solid-state DSSCs containing PC, DMF, and NMP solvents showed η's of 8.31, 6.77, and 5.74%, respectively; they all gave higher η's than those of their liquid-type DSSCs. An excellent stability was found using the quasi-solid-state DSSCs having the POE–PAI elastomer absorbed with PC-based liquid electrolyte; this cell offered up to 95% of its initial efficiency for 1000 h. It is notable that the cell with this newly designed POE–PAI elastomer hits the highest record of the η's of the quasi-solid-state DSSCs with the polymer gelator-based electrolytes. Thus, the future exploration on the functional elastomers as the polymer gelator electrolytes is a promising approach to enhance both the solar-to-electricity conversion efficiency and the long-term
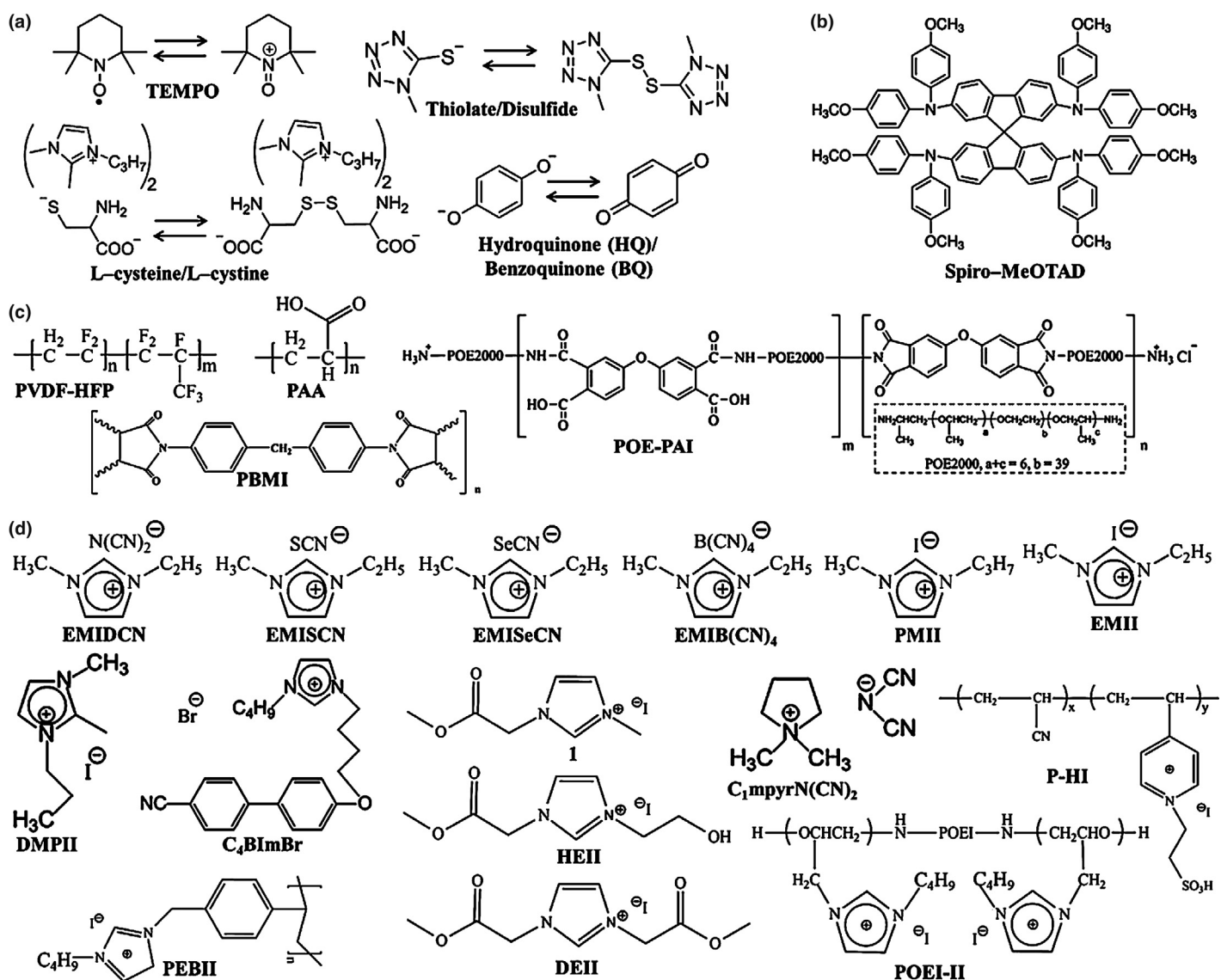
FIGURE 4

The molecular structures of (a) organic redox couple compounds, (b) organic hole transporting materials (Spiro-MeOTAD), (c) the polymer gelators, and (d) ionic liquids used for the electrolytes of DSSCs.

stability of a DSSC. The molecular structures of the abovementioned polymer gelators are shown in Fig. 4c, whereas the pertinent DSSCs' parameters are summarized in Table 3.

Ionic liquid-based electrolytes
An ionic liquid is an organic molten salt consisting of a large cation and a charge-delocalized anion. Because the noncovalent interaction lies between the cation and the anion of an ionic liquid, an ionic liquid usually has a low melting point (below 100 °C) and is usually in a liquid state. Moreover, an ionic liquid also possesses various advantages, including negligible vapor pressure, high thermal stability, wide electrochemical window, high ionic conductivity, easy preparation, and high flexibility of the construction [78,79]. Ionic liquids may undergo almost unlimited constructional variations to adapt to the specific requirements of the quasi-solid-state DSSCs; in other words, the ionic liquids can be designed to render the ionic liquid-based electrolytes with high ionic

conductivity, low viscosity, or good prohibitive ability toward back electron recombination, etc. Therefore, the ionic liquids can be used as the solvent or the redox species in the ionic liquid-based electrolytes; the employed ionic liquids in quasi-solid-state DSSCs can be classified as follows: (1) room temperature ionic liquid, (2) crystal ionic liquid, and (3) functionalized ionic liquid; the molecular structures of these ionic liquids are shown in Fig. 4c. Each type of ionic liquid and the pertinent DSSCs' performance is extensively discussed and listed in Table 3.

Room temperature ionic liquid
Wang et al. first prepared a binary-ionic liquid electrolyte consisting of 1-propyl-3-methylimidazolium iodide (PMII) and 1-methyl-3-ethylimidazolium dicyanamide (EMIDCN) to obtain an η of 6.60% [80]. Because they found that the presence of EMIDCN in the binary-ionic liquid electrolyte led to an instability of the cells, another binary-ionic liquid electrolyte composed of PMII

TABLE 3

A partial list of literature studies on the DSSCs with polymer gelator-based or ionic liquid-based electrolytes.

Electrolyte	Redox couple	Dye	η (%)	Durability (% to the initial η)	Ref.
Polymer gelator-based electrolytes: polymer gelator					
PEG	I^-/I_3^-	N3	7.22	95% (after 1000 h)	[62]
PEG/PVDF–HFP	I^-/I_3^-	N3	5.08	54% (after 480 h)	[73]
PAA–PEG–PPy	I^-/I_3^-	N3	6.30	80% (after 720 h)	[74]
PBMI	I^-/I_3^-	CYC–B6S	6.24	98% (after 500 h)[a]	[75]
POE–PAI	I^-/I_3^-	N719	9.48	95% (after 1000 h)	[76,77]
Ionic liquid-based electrolytes: room temperature ionic liquid					
EMIDCN/PMII	I^-/I_3^-	Z907	6.60	N.A.	[80]
EMISCN/PMII	I^-/I_3^-	Z907	7.00	N.A.	[81]
EMISeCN	$SeCN^-/(SeCN)_3^-$	Z907	7.50	N.A.	[82]
EMIB(CN)$_4$/PMII	I^-/I_3^-	Z907	7.60	90% (after 1000 h)[a]	[83]
Ionic liquid-based electrolytes: crystal ionic liquid					
C$_1$mpyrN(CN)$_2$/EMII	I^-/I_3^-	N719	5.01	N.A.	[84]
DMPII	I^-/I_3^-	N719	5.87	N.A.	[85]
C$_4$BImBr/PMII/EMII	I^-/I_3^-	Z907	5.07	95% (after 1000 h)	[86]
Ionic liquid-based electrolytes: functionalized ionic liquid					
Ionic conductor 1	I^-/I_3^-	MK2	6.63	100% (after 1000 h)	[87]
HEII	I^-/I_3^-	MK2	7.45	96% (after 1500 h)	[88]
DEII	I^-/I_3^-	FNE29	6.50	N.A.	[89]
P–HI	I^-/I_3^-	N3	6.95	N.A.	[90]
PEBII	I^-/I_3^-	N719	6.70	N.A.	[91,92]
POEI–II	I^-/I_3^-	N719	7.65	100% (after 1000 h)	[93]

[a] The long-term stability experiment of the DSSC was performed at ∼60 °C.

and 1-ethyl-3-methylimidazolium thiocyanate (EMISCN) rendered an η of 7.00% to its cell [81]. In addition, they developed a new and low viscosity ionic liquid of 1-ethyl-3-methylimidazolium selenocyanate (EMISeCN) as an iodine-free redox species ($SeCN^-/(SeCN)_3^-$); a high η of 7.50% was achieved [82]. This is the first report on an alternative redox couple that exceeded the performance of the iodide/triiodide redox couple in full sunlight. Kuang et al. reported a new high η record of 7.60% using a 1-ethyl-3-methyl-imidazolium tetracyanoborate (EMIB(CN)$_4$)-based binary-ionic liquid electrolyte [83]. The cell with EMIB(CN)$_4$/PMII binary-ionic liquid electrolyte maintained more than 90% of its initial efficiency under light-soaking at 60 °C for 1000 h.

Crystal ionic liquid

Armel et al. synthesized a solid-state binary-ionic liquid electrolyte containing the crystal ionic liquids of N,N-dimethyl-pyrrolidinium dicyanamide (C$_1$mpyrN(CN)$_2$) and EMII to reach a good η of 5.10% [84]. Chen et al. have developed a rather efficient crystal ionic liquid, 1,2-dimethyl-3-propylimidazolium iodide (DMPII), as the charge transfer intermediate for the solid-state DSSCs [85]. With the presence of potassium iodide (KI) and polyethylene oxide (PEO, MW = 100,000 g mol^{-1}) in the DMPII as the charge transfer auxiliary agent and the crystal growth inhibitor, respectively, the pertinent solid-state DSSC showed the highest record of 5.87%. Cao-Cen et al. synthesized the crystal ionic liquid of N-4-(4-cyanobiphenyl-40-oxy)-butyl-3-butylimidazolium bromide (C$_4$BImBr), which acted as a high light-scattering material to enhance the light-harvesting of a DSSC [86]. The solid-state DSSC with EMII/I$_2$/C$_4$BImBr/PMII electrolyte showed an η of 5.07% and possessed a good long-term stability (decay <5%) under continuous light-soaking for 1000 h (1 sun, at 25 °C).

Functionalized ionic liquid

Wang et al. synthesized an ester-substituted ionic liquid mediator, 1-(2-methoxy-2-oxylethyl)-3-methyl imidazolium iodide (denoted as 1) [87], which formed the three-dimensional ionic channel of iodides and interacted with Li$^+$ by the oxygen on the ester group, thereby resulting in fast charge transfer along the polyiodide chain. In addition, the molecular size of this ester-substituted ionic liquid permitted a deep penetration of the electrolytes into the porous TiO$_2$ thin films, which facilitated the reduction of the oxidized dye molecules and favored high photocurrent generation. Thus, the pertinent DSSC exhibited an η of 6.63% and excellent long-term stability (100% of the initial η after continuous light-soaking for 1000 h). Li et al. synthesized a novel solid-state conductive ionic liquid mediator, the hydroxyethyl and ester co-substituted imidazolium iodide (HEII) [88]. The ester functional group could significantly enhance the ionic conductivity of the ionic liquid, whereas the oxygen and hydrogen atoms on the hydroxyethyl functional group were designed to participate in hydrogen bonding, which was favorable to form a closely packed structure toward high conductivity. The solid-state DSSC with HEII electrolyte achieved a cell efficiency of 7.45%. Under continuous one sun illumination for 1000 h, the cell efficiency maintained 96% of its initial value, indicating a good long-term stability. In addition, they synthesized a double-ester-substituted imidazolium iodide, namely 1,3-di(2-methoxy-2-oxoethyl)imidazolium iodide (DEII), to simultaneously act as the electron donor and acceptor [89]. The donor (DEII) was deposited on the photoanode surface for efficient dye regeneration, while the acceptor (mixture of DEII and iodine) was deposited on the counter electrode surface for the efficient electron relay for circuit completion. The counter electrode was placed on top of the photoanode to form a close contact between the donor and acceptor, which was

then sealed into a solid device. The separation of the electron donor and acceptor of a redox couple could significantly retard the charge recombination because of the absence of I_3^- in the photo-anode; therefore, the pertinent solid-state DSSC gave an η of 6.50%. In brief, this novel device structure opened up a new way for the further enhancement of the solid-state DSSC performance by increasing the ionic conductivity of ionic liquid mediator through a molecular design. Fang et al. synthesized an acidic ionic liquid polymer, P[((3-(4-vinylpyridine) propanesulfonic acid) iodide)-co-(acrylonitrile)] (P–HI), which was composed of a copolymer chain (polyethylene and polyacrylonitrile) and a sulfonic acid group [90]. The sulfonic acid group possessed strong electronegativity, which is beneficial to form the homogeneous and continuous framework of ionic liquid polymer for enhancing the transportation of redox couples in the electrolyte. Without the addition of I_2, the solid-state DSSC containing P–HI gave an η of 6.95%. Chi et al. designed a polymeric ionic liquid, poly((1-(4-ethenylphenyl)methyl)-3-butyl-imidazolium iodide) (PEBII) [91]. A (4-ethenylphenyl)methyl functional group was anchored on 1-butylimidazolium iodide and served as the self-polymerization site and rendered good conductivity ($2.0 \times 10^{-4}\,S\,cm^{-1}$ at 25 °C) to the PEBII due to the strong π–π stacking interaction between the benzene groups. In their I_2-free solid-state DSSCs, the PEBII electrolyte could deeply penetrate into mesoporous TiO_2 film, perfectly filled the nanopores between the TiO_2 nanoparticles, and prevented the formation of cavities during solvent evaporation. Therefore, the charge transfer at the interface of dye-sensitized TiO_2 film/electrolyte and the electron lifetime within the pertinent cell were significantly improved, and an η of 6.70% was obtained [92]. Recently, Chang et al. synthesized a novel polymeric ionic liquid, poly(oxyethylene)-imide imidazolium iodide (POEI–II) [93]. A poly(oxyethylene)-segmented oligo(imide) (POEI) functional group incorporated with two 1-butylimidazolium iodide ionic liquids at both ends of POEI. The POEI possessed aromatic imides and hydrophilic POE segments with multiple dipole–dipole interaction sites, which rendered POEI–II a high solubility in aqueous solutions and in organic solvents. The POE segment in the POEI–II could chelate lithium cations (Li^+) in the electrolyte to increase the V_{OC} of a cell and enable the strong inner π–π and long-pair-π electron interactions, to enhance the ionic conductivity and the ionic diffusivity of POEI–II gel electrolyte. Consequently, the quasi-solid-state DSSC with POEI–II gel electrolyte reached a high η of 7.19% with an excellent long-term stability (100% of the initial η after continuous light soaking for 1000 h).

Advanced evolution in counter electrodes

In the development of DSSCs, challenging issues are not only to achieve a high η, but also to significantly reduce their fabrication cost. In a high-performance DSSC, the counter electrode plays an important role as an electro-catalyst to trigger the reduction of the oxidized redox species, including I_3^- of I^-/I_3^-, Co^{3+} of Co^{2+}/Co^{3+}, disulfide (T_2) of disulfide/thiolate (T_2/T^-), etc. Because the reduction of oxidized redox species is one of the rate-determining steps in a DSSC [94], an electro-catalytic material coated on the counter electrode is required to facilitate the heterogeneous charge transfer rate at the interface of counter electrode/electrolyte. In other words, the function of a good electro-catalytic material is to speed up the reduction of oxidized redox species. Because the I^-/I_3^- is

the most commonly used redox couple, several research studies focused on exploring effective electro-catalytic materials toward I_3^- reduction [95–97]. The I_3^- is strongly electron-deficient and highly reactive; a slow electro-catalytic reduction of I_3^- can lead to severe energy loss in a DSSC owing to their susceptibility for recombination reactions with the photo-induced electrons. To prevent the electron recombination and the pertinent energy loss in a DSSC, a fast reduction of I_3^- using an effective electro-catalytic material as the counter electrode is a key issue to obtain a highly efficient DSSC. In general, a counter electrode requires excellent electro-catalytic ability, good charge transfer capability, good conductivity, high corrosion resistance, and good electrochemical stability [6]. Platinum (Pt) usually works as the best electro-catalyst because of its outstanding electro-catalytic ability toward I_3^- reduction, and thus, Pt is the most frequently used counter electrode in the DSSCs. However, Pt is easily poisoned by the iodide, and thereby limits the long-term stability of the counter electrode and even that of the pertinent DSSC [95–97]. Moreover, Pt is an expensive noble metal and is rare on earth. The fabrication of a highly efficient Pt film often requires an expensive high-temperature sintering oven (thermal decomposition method) or a vacuum equipment (sputtering method). Therefore, it is of no doubt that the fabrication of the counter electrodes with the other cheaper materials is definitely one of the key issues to enhance the cell efficiency of DSSCs, prolong the stability of DSSCs, and cost-down the commercialized DSSC, especially for large-scale production. In the past 10 years, several researchers dedicate themselves to develop substitutions of Pt [95–97], including (1) non-Pt metal-based, (2) transition metallic compound-based, (3) conducting polymer-based, and (4) carbonaceous-based materials. In the case of non-Pt metal-based materials, including Au, Ag, Cu, or Ni, some of them cause unfavorable side reactions with iodides or are corrosive in the iodide electrolytes or possess a low catalytic activity toward I_3^- reduction. Therefore, non-Pt metal-based materials rarely render good η's (<5%) to their DSSCs. With regard to transition metallic compound-based materials, many of them contain heavy metals and are often synthesized using several complicated procedures including a high-cost vacuum annealing process. In addition, transition metallic compound-based materials generally offered their DSSCs the η's of 5–7%, which are approximately 80–90% to the η of their Pt-based DSSCs. In the case of conducting polymer-based and carbonaceous-based materials, they were reported as the promising replacements for Pt due to their excellent electro-catalytic ability, high electrical conductivity, low cost (consisting of earth-abundant elements), and good electrochemical stability for the regeneration of the redox species; consequently, the conducting polymer-based and carbonaceous-based counter electrodes were considered as the most promising Pt-free counter electrodes for DSSCs, and they usually reached high η's of 7–9%, even higher than those of their Pt-based DSSCs. In Sections 'Conducting polymer-based counter electrodes' and 'Carbonaceous-based counter electrodes', we present a brief overview on the highly efficient conducting polymer-based and carbonaceous-based materials as the counter electrodes for DSSCs with cell efficiencies >7%, respectively. The structures of these highly efficient conducting polymer-based and carbonaceous-based materials are shown in Fig. 5; the photovoltaic parameters of the pertinent DSSCs are summarized in Tables 4 and 5, respectively.

(a)

(b)
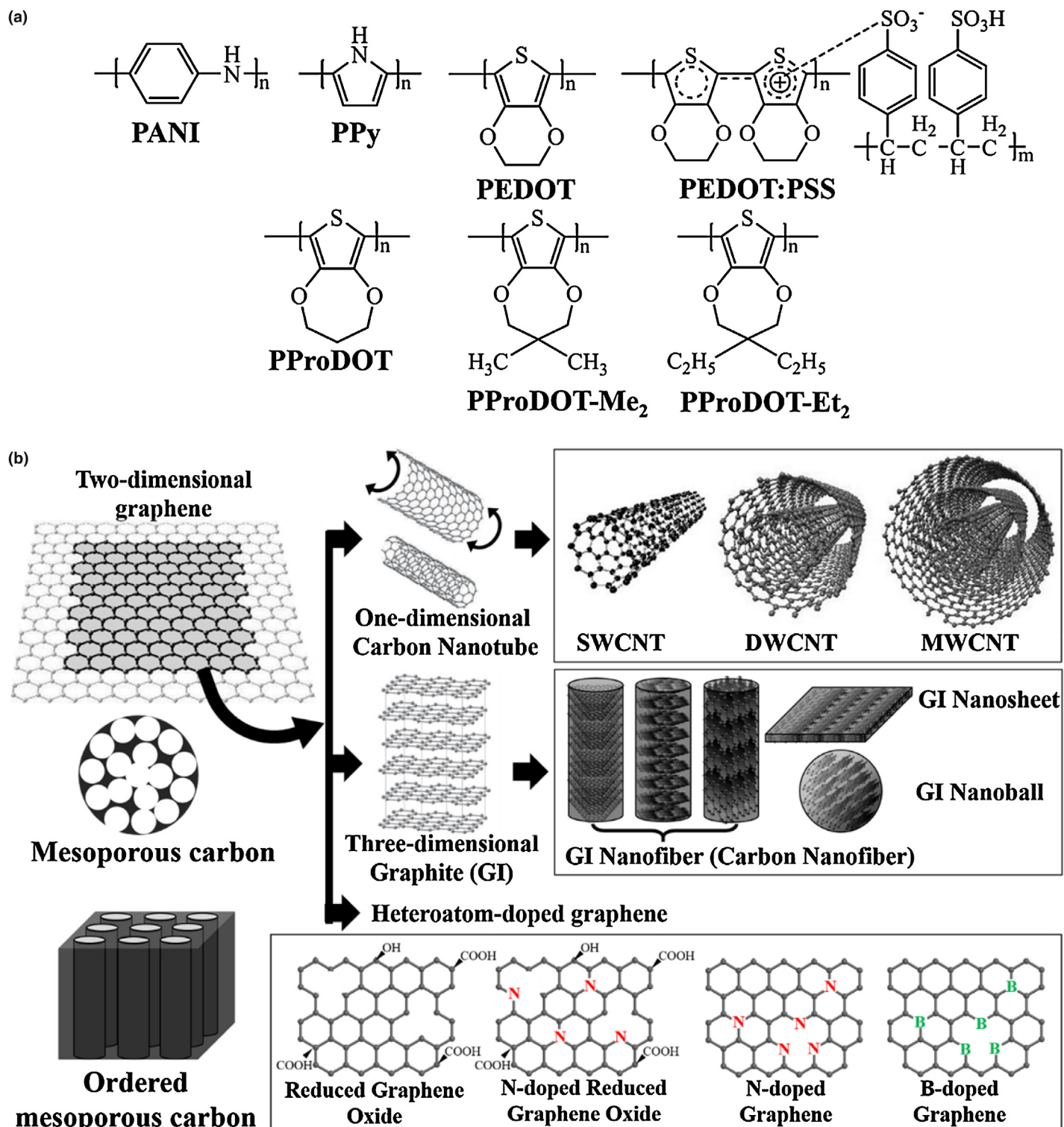
FIGURE 5

Schematic sketches of (a) the conducting polymers type and (b) carbonaceous type materials for the counter electrodes of DSSCs.

Conducting polymer-based counter electrodes

Conducting polymers are known as the organic conductors, which can conduct the electrons using their conjugated polymer chains. The high transparency of the conducting polymers benefits the development of the bifacial DSSCs illuminated from both sides of the cells, implying that the conducting polymers have a great flexibility for the multiple applications in DSSCs. Thus far, several

highly efficient conducting polymers have been developed, for example, polyaniline (PANI), polypyrrole (PPy), poly(3,4-ethylene-dioxythiophene) (PEDOT), poly(3,4-ethylenedioxythiophene):poly(styrenesulfonate) (PEDOT:PSS), sulfonated-poly(thiophene-3-[2-(2-methoxyethoxy)-ethoxy]-2,5-diyl) (s-PT), poly(3,4-propylene-dioxythiophene) (PProDOT), poly(3,3-dimethyl-3,4-dihydro-2H-thieno(3,4-b)(1,4)dioxepine) (PProDOT-Me$_2$), poly(3,3-diethyl-3,

TABLE 4

A partial list of literature studies on the DSSCs with conducting polymer-based counter electrodes.

Counter electrode	Redox couple	Dye	η (%)	η of Pt (%)	Ref.
Conducting polymer-based counter electrodes: aniline type					
PANI	I^-/I_3^-	N719	7.15	6.90	[98]
4-ATP-doped PANI	I^-/I_3^-	N719	8.35	7.46	[99]
H_2SO_4-doped PANI	I^-/I_3^-	N719	7.30	N.A.	[89]
SDS-doped PANI	I^-/I_3^-	N719	7.00	7.40	[100]
I_2-doped PANI emeraldine salt	I^-/I_3^-	N719	7.86	N.A.	[101]
PANI nanowire	I^-/I_3^-	N719	7.24	7.98	[102]
Oriented PANI nanowire array	Co^{2+}/Co^{3+}	FNE29	8.24	6.78	[103]
Conducting polymer-based counter electrodes: pyrrole type					
PPy	I^-/I_3^-	N719	7.66	6.90	[104]
HCl-doped PPy	I^-/I_3^-	N719	7.73	8.20	[105]
PPy/PEDOT:PSS	I^-/I_3^-	N719	7.60	7.73	[106]
Conducting polymer-based counter electrodes: thiophene type					
s-PT	I^-/I_3^-	N719	8.45	8.07	[107]
PEDOT	I^-/I_3^-	N719	8.50	8.75	[108]
PEDOT:PSS			8.33		
PProDOT	I^-/I_3^-	N3	7.08	7.77	[109]
PProDOT–Et$_2$			7.88		
BMITFSI-doped PEDOT	I^-/I_3^-	N719	7.93	8.71	[111]
HMIBF$_4$-doped PEDOT	I^-/I_3^-	N719	7.78	8.09	[112]
DMIBF$_4$-doped PEDOT			7.20		
HMIPF$_6$-doped PEDOT			8.28		
HMISO$_3$CF$_3$-doped PEDOT			7.82		
HMITFSI-doped PEDOT			8.87		
BMITFSI-doped PProDOT	I^-/I_3^-	N719	9.12	9.53	[113]
BMPyTFSI-doped PProDOT			9.12		
EMIFAP-doped PProDOT			9.25		
PEDOT nanofiber	I^-/I_3^-	N719	8.30	8.60	[114]
PEDOT hollow microflower array	I^-/I_3^-	N719	7.20	7.61	[115]
Nanopatterned PEDOT (on PS/PET)	I^-/I_3^-	N719	7.10	7.60	[116]
SDS-doped PEDOT nanofiber	I^-/I_3^-	N719	9.20	8.60	[114]
PEDOT	Co^{2+}/Co^{3+}	Y123	8.62	8.24	[117]
PProDOT–Me$_2$			8.74		
PProDOT–Et$_2$			8.00		
BMITFSI-doped PProDOT			9.90		
EMIFAP-doped PProDOT			8.70		
PProDOT	Co^{2+}/Co^{3+}	Y123	10.08	9.52	[118]
PEDOT:PSS (on Ag/PET)	Co^{2+}/Co^{3+}	Y123	7.00	6.90	[119]
PEDOT	T_2/T^-	Z907	7.90	5.60	[120]

4-dihydro-2*H*-thieno-(3,4-*b*)(1,4)dioxepine) (PProDOT-Et$_2$), etc. (Fig. 5a); they are often synthesized by simple electro-polymerization processes. The as-prepared conducting polymer films often show the microstructures of three-dimensional matrix or dense thin layer; the former lacks directional and fast electron pathways, the latter leads to the insufficient electrochemical surfaces. In this regard, many approaches are developed: (Case I) synthesize functionalized conducting polymers through various chemical dopants to enhance the conjugation of the conducting polymers or to increase the active sites of the conducting polymers; (Case II) design different morphologies of conducting polymers to give large surface areas or directional electron pathways. Considering the molecular constructions of the polymer main chains of various conducting polymers, they can be simply divided into three categories: (1) aniline type, (2) pyrrole type, and (3) thiophene type; the pertinent DSSCs' parameters for each group are listed in Table 4.

Aniline type

Aniline type conducting polymers included few analogs, and the simple format of polyaniline (PANI, $\eta = 7.15\%$) [98] showed the good performance as a counter electrode for DSSCs. PANI was also reported as a transparent counter electrode for bifacial DSSCs to achieve good η's from the front-side (6.70%), rear-side (4.15%), and both-side (8.35%, the highest record for PANI-based counter electrodes) using a 4-aminothiophenol (4-ATP)-incorporated electrochemical deposition process (the obtained film is denoted as 4-ATP-doped PANI) [99]. To further enhance the η's of the PANI-based DSSCs under the front-side illumination, various chemical dopants were used to incorporate or embed with PANI polymer chain to enhance the conjugation of PANI, including H_2SO_4-doped PANI (7.30%) [89], sodium dodecyl sulfate-doped PANI (SDS-doped PANI, 7.00%) [100], iodine vapor-doped PANI emeraldine salt nanoparticle (7.86%, note that the dopants for this film actually include Cl$^-$, and n-dodecyl sulfate ($C_{12}H_{25}$-SO$_4^{2-}$), I_3^-,

TABLE 5

A partial list of literature studies on the DSSCs with carbonaceous-based counter electrodes.

Counter electrode	Redox couple	Dye	η (%)	η of Pt (%)	Ref.
Carbonaceous-based counter electrodes: sp^2 type					
GN	I^-/I_3^-	N719	8.19	8.89	[122]
Honeycomb-like GN	I^-/I_3^-	N719	7.80	8.00	[123]
GI NB	I^-/I_3^-	N719	7.88	8.38	[125]
Carbon nanofiber	I^-/I_3^-	N719	7.00	7.10	[126]
Hollow carbon nanofiber	I^-/I_3^-	N719	7.21	7.69	[127]
SWCNT	I^-/I_3^-	N719	7.61	8.49	[128]
DWCNT			8.03		
MWCNT	I^-/I_3^-	N719	9.34	9.09	[129]
RGO	I^-/I_3^-	C106	9.54	9.14	[103]
N-doped GN	I^-/I_3^-	N719	7.18	7.58	[130]
N-doped RGO	I^-/I_3^-	N3	8.03	7.33	[131]
GN	Co^{2+}/Co^{3+}	Y123	9.30	8.10	[132]
B-doped GN	Co^{2+}/Co^{3+}	JK-303	9.21	8.45	[133]
N-doped GN	Co^{2+}/Co^{3+}	O-alkylated-JK-225	9.05	8.43	[134]
Carbonaceous-based counter electrodes: sp^3 type					
Carbon black	I^-/I_3^-	N719	9.10	N.A.	[135]
Carbon dye	I^-/I_3^-	N719	7.50	7.50	[121]
Mesoporous carbon	I^-/I_3^-	N719	7.01	7.76	[136]
Ordered mesoporous carbon	I^-/I_3^-	N719	7.50	7.50	[121]
Rosin carbon	I^-/I_3^-	N719	7.00	8.37	[137]

and I_5^-) [101] etc. To increase the surface areas, PANI were synthesized with various structures, for example, PANI nanowire (7.24%) [102], and one-dimensional bottom-up PANI nanowire array (8.24%, for Co^{2+}/Co^{3+} redox couple) [103].

Pyrrole type
Pyrrole type conducting polymer only contains PPy (η = 7.66%) [104]. To further enhance the η's of the PPy-based DSSCs, various chemical dopants were used to incorporate or embed with PPy polymer chain to enhance the conjugation of PPy, for example, HCl-doped discrete spherical PPy nanoparticle (7.73%) [105]. Because PPy nanoparticles usually have poor adhesion to the substrate, another water soluble conducting polymer, PEDOT:PSS, is used to anchor the PPy nanoparticle on the substrate; the pertinent composite film of PPy/PEDOT:PSS (7.60%) [106] rendered good η to its DSSC.

Thiophene type
Thiophene-type conducting polymers include sulfonated-poly(-thiophene-3-[2-(2-methoxyethoxy)-ethoxy]-2,5-diyl) (s-PT, 8.45%) [107], PEDOT (8.50%), PEDOT:PSS (8.33%) [108], PProDOT (7.08%), and PProDOT–Et$_2$ (7.88%) [109] etc. Among them, PEDOT and PEDOT:PSS were the most frequently used conducting polymers, and both of them were often prepared as the transparent or flexible counter electrodes to provide multiple applications and good η's to their DSSCs [107,110]. To further enhance the η's of the thiophene-based DSSCs, various chemical dopants were used to incorporate or embed with the polymer chains to enhance the conjugation of thiophene-based conducting polymers, including 1-butyl-3-methylimidazolium bis(trifluoromethylsulfonyl)imide-doped PEDOT (BMITFSI-doped PEDOT, 7.93%) [111], 1-hexyl-3-methylimidazolium tetrafluoroborate-doped PEDOT (HMIBF$_4$-doped PEDOT, 7.78%), 1-dectyl-3-methylimidazolium tetrafluoroborate-doped PEDOT (DMIBF$_4$-doped PEDOT, 7.20%), 1-hexyl-3-methylimidazolium hexafluorophosphate-doped PEDOT (HMIPF$_6$-doped PEDOT,

8.28%), 1-hexyl-3-methylimidazolium trifluoromethansulfonate-doped PEDOT (HMISO$_3$CF$_3$-doped PEDOT, 7.82%), 1-hexyl-3-methylimidazolium bis(trifluoromethylsulfonyl)imide-doped PEDOT (HMITFSI-doped PEDOT, 8.87%) [112], BMITFSI-doped PProDOT (9.12%), 1-butyl-3-methylpyridnium bis(trifluoromethylsulfonyl)imide-doped PProDOT (BMPyTFSI-doped PProDOT, 9.12%), 1-ethyl-3-methylimidazolium tris(pentafluoroethyl)trifluorophosphate-doped PProDOT (EMIFAP-doped PProDOT, 9.25%) [113], etc. To increase the surface areas, thiophene-type conducting polymers were synthesized with various structures, for example, PEDOT nanofiber (8.30%) [114], PEDOT hollow microflower array (7.20%) [115], nano-patterned PEDOT on polystyrene/polyethylene terephthalate (PS/PET) (7.10%) [116], etc. For PEDOT, the combination of the chemically doped PEDOT and nanostructured PEDOT (i.e., sodium dodecyl sulfate-doped PEDOT nanofiber (SDS-doped PEDOT nanofiber)) brings the highest record of 9.20% [114] to the cells with PEDOT-based counter electrodes using I^-/I_3^- electrolyte to date; thus, it is a convincing strategy to design a chemically doped and nanostructured conducting polymer as a highly efficient counter electrode for DSSCs. In addition, thiophene-type conducting polymers also showed great electro-catalytic ability toward Co^{2+}/Co^{3+} redox couple, thin films of PEDOT (8.62%), PProDOT-Me$_2$ (8.74%), PProDOT-Et$_2$ (8.00%), BMITFSI-doped PProDOT (9.90%), EMIFAP-doped PProDOT (8.70%) [117], PProDOT (10.08%) [118], and PEDOT:PSS on a honeycomb-structured Ag grid/polyethylene terephthalate substrate (7.00%) [119], etc. reached good η's of their DSSCs. With disulfide/thiolate (T$_2$/T$^-$) redox couple, PEDOT thin film achieved a good η up 7.90% to its DSSC [120] and even delivered more stable performance than the Pt-based DSSC.

Carbonaceous-based counter electrodes
Several carbonaceous materials have become potential alternatives to substitute Pt because of their extremely low cost and good electrochemical properties. In general, carbonaceous-based

materials are constructed by the carbon atoms connected with a sp^2 planar or a sp^3 tetrahedron arrangement. The most attractive sp^2 planar-arranged carbonaceous material is graphite (GI) because of its metal-like conductivity. Therefore, several GI-derived materials were extensively explored [121], such as graphene (GN), graphene oxide (GO), reduced graphene oxide (RGO), SWCNT, MWCNT, carbon nanofiber, etc. On the other hand, many sp^3 tetrahedron-arranged carbonaceous materials were also studied as the counter electrodes for DSSCs [121], for example, activated carbon, carbon black, conductive carbon, carbon dye, ordered mesoporous carbon, discarded toner of a printer, etc. However, dispersants of carbonaceous materials were always used to prepare the crack-free carbon-based electro-catalytic film on the conducting substrate. Thus, the electro-catalytic ability and conductivity of the carbonaceous type counter electrode would be limited by the addition of the dispersants. Here, various carbonaceous materials are briefly divided into two groups: (1) sp^2-type and (2) sp^3-type; the schematic structures of these carbonaceous materials are shown in Fig. 5b, while the pertinent DSSCs' data are listed in Table 5.

sp^2 type

The sp^2-type carbonaceous materials normally possess orientated charge transfer pathways and thus excellent conductivity. First, two-dimensional charge transfer pathways can be provided by the sheet-like GN (8.19%) [122], honeycomb-like GN (7.80%) [123], etc. As shown in Fig. 5b, the two-dimensional GN can be stacked into three-dimensional GI or rolled into one-dimensional nanotubes [124]. In the case of three-dimensional GI, various structures of GI can be formed by varying different stacking modes of GI, as shown in Fig. 5b; GI nanofiber (3.60%), GI nanosheet (2.99%), and GI nanoball (7.88%) were investigated as the counter electrode of DSSCs [125]. In addition, GI nanofibers were also known as the carbon nanofiber; the carbon nanofiber (7.00%) [126] and hollow carbon nanofiber (7.21%) [127] were reported as the efficient electro-catalysts for the counter electrodes of DSSCs. In the case of one-dimensional nanotubes, SWCNT (7.61%), double-walled nanotubes (DWCNT, 8.03%) [128], MWCNT (9.34%) [129], etc. were investigated to give good η's. However, the electro-catalytic active sites of GI-based materials are located on the sp^2 edges or inner defects on the sp^2 plane, this explains why the η's of the pertinent DSSCs are rather limited. Recently, heteroatoms, for example, oxide (O), boron (B) or nitride (N), are incorporated into the sp^2 planes of those graphite-based materials to enhance their electro-catalytic ability, for example, RGO (9.54%) [103], N-doped GN (7.18%) [130], and N-doped RGO (8.03%) [131]. Moreover, with the incorporation of the Co^{2+}/Co^{3+} redox couple, films of GN (9.30%) [132], B-doped GN (9.21%) [133], and N-doped GN (9.05%) [134], etc., rendered impressive η's to their cells. The inserted heteroatoms cause several defects on graphene, and render additional lone pair electrons or holes to the delocalized π–π orbital of GN. Thus, the inserted heteroatoms in GN function as the electro-catalytic active sites for the redox reaction. However, it should be noticed that the inserted heteroatoms simultaneously result in local strains in the hexagonal carbon network of GN, leading to the structural deformations of GN's π–π orbital, thus decreasing the conductivity of GN. In brief, the balance between the electro-catalytic active sites on GN and the conductivity of GN

should be achieved by adjusting the amount of inserted heteroatoms [134].

sp^3 type

The sp^3-type carbonaceous materials normally possess sufficient electro-catalytic active sites but lack of good conductivity because of the nonoriented charge transfer pathways. Thus far, carbon black (9.10%) [135], carbon dye (7.50%) [121], mesoporous carbon (7.01%) [136], ordered mesoporous carbon (7.50%) [121], rosin carbon (7.00%) [137], etc. have been proposed as the potential electro-catalysts for the counter electrodes of DSSCs.

Summary and future outlook

In the past two decades, great progresses have been made for the DSSCs, particularly on the performance, durability, and cost saving, by incorporating various organic materials in cell fabrications. Accordingly, this review briefly summarized the recent progresses on the DSSCs with organic material-modified TiO_2 electrodes, organic dyes, polymer gel/ionic liquid electrolytes, and metal element-free electrocatalytic films. To prepare organic material-modified TiO_2 electrodes, some polymers were investigated and used as the binder, dispersant, and template to prepare the functional TiO_2 films with high surface area, suitable pore size, and light-scattering effect; moreover, several carbonaceous materials (i.e., CNTs and graphene) were added into the TiO_2 films to significantly improve their electrical conductivity. In the development of organic dyes, the DSSC with a perylene dye, namely C275 dye, reached a new milestone of the η (12.50%), which demonstrated that the organic dye-based DSSC can achieve an η as good as Ru dye-based cell. On the other hand, a squaraine-based near-infrared sensitizer, DTS-CA dye, with a maximum absorption peak at 667 nm was synthesized for the DSSC to harvest the solar spectrum up to the near-infrared region, and it exhibited an excellent η of 8.90%. Because the photocurrent response of DSSCs depends mainly on the sensitizing ability of dyes, the co-sensitization method using multiple dyes with compensatory absorption spectra could be a convenient approach to extend the absorption threshold of the sensitizers in the visible and near-infrared regions of the solar spectrum. By using quasi-solid-state ionic type electrolytes (polymer gelator and ionic liquid electrolytes) in DSSCs, the long-term stability of the pertinent cells was highly improved compared to that of the traditional DSSCs with liquid electrolytes. When the POE–PAI elastomer was used as the polymer matrix for the electrolyte, the corresponding DSSC offered a superior cell stability and exhibited higher η (9.48%) than that of the cell using the liquid electrolyte (8.84%). Despite the fact that DSSCs with ionic liquid electrolytes show superior long-term stability than that of the cell with liquid electrolytes, the former system possesses relatively low cell efficiency (<8%) compared to the latter; indeed, the cell efficiency of the former needs to be further improved because both stability and efficiency are the two essential criteria for a good DSSC. The current challenge in ionic liquids-based quasi-solid-state DSSCs is focused on how to lower the viscosity of the ionic liquids and to enhance the diffusion rate of the redox couples, which would be a key issue for the future study of ionic liquids electrolytes. Thus far, metal element-free electro-catalytic films based on conducting polymers (i.e., PANI, PPy, PEDOT, PProDOT, and PProDOT–Et_2, etc.) and carbonaceous materials

(i.e., GN, GI, CNTs, RGO, carbon nanofiber, carbon black, etc.) have been successfully developed as the highly efficient counter electrode for Pt-free DSSCs, and most of them show better electro-catalytic activity toward I_3^- reduction than Pt film. The DSSCs with these metal element-free electro-catalytic films thus exhibited superior cell performance than that of the cell with a Pt film. The concurrent advantage in low-cost materials and high performance for the Pt-free DSSCs using these metal element-free electro-catalytic films would allow the promising future of DSSCs for mass production, and render DSSCs to be more competitive among various photovoltaic devices in the solar cell markets.

It is well known that there are still several factors limiting the practical uses of DSSCs. In the future, scientists and engineers need to optimize every material within the DSSC to further achieve a breakthrough on the performance and to preserve its durability. With more efforts devoted to DSSCs, it is likely that the commercialization of DSSCs will be realized within a few years. Thus far, undoubtedly, the development and utilization of organic materials for constructing each part of DSSCs is one of the most important contributions to the full success in this field.

Acknowledgment

References

[1] B. O'Regan, M. Grätzel, Nature 353 (1991) 737–740.
[2] A. Hagfeldt, M. Grätzel, Acc. Chem. Res. 33 (2000) 269–277.
[3] F. Gao, et al. J. Am. Chem. Soc. 130 (2008) 10720–10728.
[4] S. Mathew, et al. Nat. Chem. 6 (2014) 242–247.
[5] K. Kakiage, et al. Chem. Commun. 51 (2015) 15894–15897.
[6] M. Ye, et al. Mater. Today 18 (2015) 155–162.
[7] J. Li, et al. Langmuir 25 (2009) 11162–11167.
[8] K.M. Lee, et al. Sol. Energy Mater. Sol. Cells 90 (2006) 2398–2404.
[9] Y. Saito, et al. Sol. Energy Mater. Sol. Cells 83 (2004) 1–13.
[10] Z. Liu, et al. Thin Solid Films 484 (2005) 346–351.
[11] K.H. Park, C.K. Hong, Electrochem. Commun. 10 (2008) 1187–1190.
[12] S.H. Ahn, et al. J. Mater. Chem. 21 (2011) 1772–1779.
[13] J.H. Pan, et al. Chem. Eng. J. 170 (2011) 363–380.
[14] Z. Sun, et al. J. Mater. Chem. 22 (2012) 11711–11719.
[15] S. Agarwala, et al. ACS Appl. Mater. Interfaces 2 (2010) 1844–1850.
[16] P. Docampo, et al. Adv. Funct. Mater. 20 (2010) 1787–1796.
[17] S. Guldin, et al. Small 8 (2012) 432–440.
[18] D.J. Kim, et al. Phys. Chem. Chem. Phys. 15 (2013) 7345–7353.
[19] J.H. Lee, et al. J. Power Sources 298 (2015) 14–22.
[20] S. Hore, et al. Chem. Commun. (2005) 2011–2013.
[21] K.M. Lee, et al. Sol. Energy Mater. Sol. Cells 93 (2009) 2003–2007.
[22] K.M. Lee, et al. Sol. Energy Mater. Sol. Cells 92 (2008) 1628–1633.
[23] T. Sawatsuk, et al. Diamond Relat. Mater. 18 (2009) 524–527.
[24] P. Brown, et al. J. Phys. Chem. C 112 (2008) 4776–4782.
[25] N. Yang, et al. ACS Nano 4 (2010) 887–894.
[26] C.P. Lee, et al. RSC Adv. 5 (2015) 23810–23825.
[27] S. Ahmad, et al. Energy Environ. Sci. 6 (2013) 3439–3466.
[28] Y.S. Yen, et al. J. Mater. Chem. 22 (2012) 8734.
[29] W. Zeng, et al. Chem. Mater. 22 (2010) 1915–1925.
[30] Y. Bai, et al. J. Am. Chem. Soc. 133 (2011) 11442–11445.
[31] M. Xu, et al. Energy Environ. Sci. 4 (2011) 4735–4742.
[32] H. Lai, et al. RSC Adv. 2 (2012) 2427–2432.
[33] C. Chen, et al. RSC Adv. 2 (2012) 7788–7797.
[34] W. Zhu, et al. Adv. Funct. Mater. 21 (2011) 756–763.
[35] Y. Wu, et al. Adv. Energy Mater. 2 (2012) 149–156.
[36] Y. Wu, et al. Energy Environ. Sci. 5 (2012) 8261–8272.
[37] S. Qu, et al. Chem. Commun. 48 (2012) 6972–6974.
[38] J. He, et al. Chem. Eur. J. 18 (2012) 7903–7915.
[39] A. Dessi, et al. Chem. Commun. 50 (2014) 13952–13955.
[40] H.H. Chou, et al. J. Mater. Chem. 22 (2012) 10929–10938.

[41] Y. Cui, et al. Chem. Mater. 23 (2011) 4394–4401.
[42] C.H. Chen, et al. Chem. Eur. J. 16 (2010) 3184–3193.
[43] J.H. Chen, et al. J. Org. Chem. 76 (2011) 8977–8985.
[44] L.Y. Lin, et al. J. Mater. Chem. 21 (2011) 5950–5958.
[45] K. Pei, et al. Chem. Eur. J. 18 (2012) 8190–8200.
[46] S.R. Li, et al. Chem. Eur. J. 18 (2012) 12085–12095.
[47] S.R. Li, et al. Tetrahedron 70 (2014) 6276–6284.
[48] Z. Yao, et al. Angew. Chem. Int. Ed. 54 (2015) 5994–5998.
[49] Z. Yao, et al. J. Am. Chem. Soc. 137 (2015) 3799–3802.
[50] S. Paek, et al. Chem. Commun. 47 (2011) 2874–2876.
[51] F.M. Jradi, et al. Chem. Mater. 27 (2015) 2480–2487.
[52] Y. Hao, et al. Chem. Commun. (2009) 4031–4033.
[53] Y. Hao, et al. ChemSusChem 4 (2011) 1601–1605.
[54] X.F. Wang, et al. J. Power Sources 242 (2013) 860–864.
[55] E. Stathatos, et al. Chem. Mater. 15 (2003) 1825–1829.
[56] Z. Zhang, et al. Adv. Funct. Mater. 18 (2008) 341–346.
[57] M. Wang, et al. Nat. Chem. 2 (2010) 385–389.
[58] M. Cheng, et al. Energy Environ. Sci. 5 (2012) 6290–6293.
[59] M. Cheng, et al. Angew. Chem. Int. Ed. 51 (2012) 9896–9899.
[60] G.R.A. Kumara, et al. Chem. Mater. 14 (2002) 954–955.
[61] U. Bach, et al. Nature 395 (1998) 583–585.
[62] J.H. Wu, et al. Adv. Funct. Mater. 17 (2007) 2645–2652.
[63] P. Wang, et al. J. Am. Chem. Soc. 125 (2003) 1166–1167.
[64] G. Hodes, D. Cahen, Acc. Chem. Res. 45 (2012) 705–713.
[65] I. Chung, et al. Nature 485 (2012) 486–489.
[66] J. Bouclé, J. Ackermann, Polym. Int. 61 (2012) 355–373.
[67] J. Burschka, et al. Nature 499 (2013) 316–319.
[68] A. Kojima, et al. J. Am. Chem. Soc. 131 (2009) 6050–6051.
[69] H. Zhou, et al. Science 345 (2014) 542–546.
[70] M. Saliba, et al. Energy Environ. Sci. 9 (2016) 1989–1997.
[71] J.W. Choi, et al. Solid State Ionics 178 (2007) 1235–1241.
[72] H. Yang, et al. Mater. Chem. Phys. 110 (2008) 38–42.
[73] J. Zhang, et al. Electrochim. Acta 53 (2008) 5415–5422.
[74] Z. Lan, et al. Energy Environ. Sci. 2 (2009) 524–528.
[75] J.G. Chen, et al. J. Phys. Chem. C 114 (2010) 13832–13837.
[76] R.X. Dong, et al. J. Mater. Chem. A 1 (2013) 8471–8478.
[77] S.Y. Shen, et al. ACS Appl. Mater. Interfaces 6 (2014) 18489–18496.
[78] J.M. Pringle, et al. J. Mater. Chem. 12 (2002) 3475–3480.
[79] C.P. Fredlake, et al. J. Chem. Eng. Data 49 (2004) 954–964.
[80] P. Wang, et al. J. Phys. Chem. B 107 (2003) 13280–13285.
[81] P. Wang, et al. Chem. Mater. 16 (2004) 2694–2696.
[82] P. Wang, et al. J. Am. Chem. Soc. 126 (2004) 7164–7165.
[83] D. Kuang, et al. Small 3 (2007) 2094–2102.
[84] V. Armel, et al. Energy Environ. Sci. 4 (2011) 2234–2239.
[85] J. Chen, et al. J. Mater. Chem. 21 (2011) 16448–16452.
[86] H. Cao-Cen, et al. J. Mater. Chem. 22 (2012) 12842–12850.
[87] H. Wang, et al. Adv. Mater. 24 (2012) 121–124.
[88] J. Li, et al. Chem. Commun. 49 (2013) 9446–9448.
[89] P. Xu, et al. Electrochim. Acta 125 (2014) 163–169.
[90] Y. Fang, et al. Electrochem. Commun. 13 (2011) 60–63.
[91] W.S. Chi, et al. Electrochem. Commun. 13 (2011) 1349–1352.
[92] D.K. Roh, et al. J. Mater. Chem. 22 (2012) 11079–11085.
[93] L.Y. Chang, et al. J. Mater. Chem. A 2 (2014) 20814–20822.
[94] A. Listorti, et al. Chem. Mater. 23 (2011) 3381–3399.
[95] M. Wu, et al. J. Am. Chem. Soc. 134 (2012) 3419–3428.
[96] M. Wu, T. Ma, ChemSusChem 5 (2012) 1343–1357.
[97] S. Yun, et al. Adv. Mater. 26 (2014) 6210–6237.
[98] Q. Li, et al. Electrochem. Commun. 10 (2008) 1299–1302.
[99] J. Wu, et al. Sci. Rep. 4 (2014) 4028.
[100] Y. Qiu, et al. J. Power Sources 253 (2014) 300–304.
[101] Y.W. Lee, et al. Synth. Met. 174 (2013) 6–13.
[102] T.T. Duong, et al. Curr. Appl. Phys. 14 (2014) 1607–1611.
[103] X. Xu, et al. Sci. Rep. 3 (2013) 1489.
[104] J. Wu, et al. J. Power Sources 181 (2008) 172–176.
[105] S.S. Jeon, et al. J. Mater. Chem. 21 (2011) 8146.
[106] G. Yue, et al. J. Phys. Chem. C 116 (2012) 18057–18063.
[107] C.T. Li, et al. J. Mater. Chem. A 3 (2015) 24479–24486.
[108] T.L. Zhang, et al. J. Mater. Chem. A 1 (2013) 1724–1730.
[109] K.M. Lee, et al. J. Power Sources 188 (2009) 313–318.
[110] S. Ahmad, et al. Chem. Commun. 48 (2012) 9714–9716.
[111] S. Ahmad, et al. J. Mater. Chem. 20 (2010) 1654–1658.
[112] C.T. Li, et al. Nano Energy 9 (2014) 1–14.
[113] S. Ahmad, et al. ChemPhysChem 11 (2010) 2814–2819.

[114] T.H. Lee, et al. J. Mater. Chem. 22 (2012) 21624–21629.
[115] C.W. Kung, et al. J. Mater. Chem. A 1 (2013) 10693–10702.
[116] J. Kwon, et al. Nanoscale 5 (2013) 7838–7843.
[117] S. Ahmad, et al. Phys. Chem. Chem. Phys. 14 (2012) 10631–10639.
[118] J.H. Yum, et al. Nat. Commun. 3 (2012) 631.
[119] J. Idígoras, et al. J. Mater. Chem. A 2 (2014) 3175–3181.
[120] J. Burschka, et al. Energy Environ. Sci. 5 (2012) 6089–6097.
[121] M. Wu, et al. Energy Environ. Sci. 4 (2011) 2308–2315.
[122] M.H. Yeh, et al. Carbon 50 (2012) 4192–4202.
[123] H. Wang, et al. Angew. Chem. Int. Ed. 52 (2013) 9210–9214.
[124] L.J. Brennan, et al. Adv. Energy Mater. 1 (2011) 472–485.
[125] Y.Y. Li, et al. Electrochim. Acta 179 (2015) 211–219.

[126] G. Veerappan, et al. J. Power Sources 196 (2011) 10798–10805.
[127] S.H. Park, et al. J. Power Sources 239 (2013) 122–127.
[128] D. Zhang, et al. Microchim. Acta 174 (2011) 73–79.
[129] J. Balamurugan, et al. RSC Adv. 3 (2013) 4321–4331.
[130] P. Zhai, et al. Small 10 (2014) 3347–3353.
[131] X. Zhang, et al. RSC Adv. 3 (2013) 9005–9010.
[132] L. Kavan, et al. ACS Nano 5 (2011) 9171–9178.
[133] S.M. Jung, et al. Chem. Mater. 26 (2014) 3586–3591.
[134] M.J. Ju, et al. ACS Nano 7 (2013) 5243–5250.
[135] T.N. Murakami, et al. J. Electrochem. Soc. 153 (2006) A2255–A2261.
[136] M. Wu, et al. J. Mater. Chem. 22 (2012) 11121–11127.
[137] L. Wang, et al. Chem. Commun. 50 (2014) 1701–1703.

RESEARCH: Review